Supplementary Materials For

A Multi-faceted Experimental Study on the Dynamic Behavior of $MgSiO_3$ Glass in the Earth's Deep Interior.

Young Jay Ryu[1,*], Yanbin Wang[1], Tony Yu[1], Fiona Bonnet[1,†], Eran Greenberg[1,††], Clemens Prescher[2], Vitali B. Prakapenka[1], Sergey Tkachev[1], Peter Eng[1], Joanne E. Stubbs[1], Przemyslaw Dera[3], Heather Watson[4], and Mark L. Rivers[1]

[1]Center for Advanced Radiation Sources, The University of Chicago, Chicago, IL 60637, USA.

[2]Institute of Earth and Environmental Sciences, Albert-Ludwigs-Universität Freiburg, Freiburg, D-79104, Germany.

[3]Hawai'i Institute of Geophysics and Planetology, University of Hawai'i Mānoa, Hawai'i, HI, 96822, USA.

[4]Department of Physics and Astronomy, Union College, Schenectady, NY 12308, USA.

[†]Currently at the Laboratoire de Science de la Terre, CNRS UMR 5570, ENS Lyon, 46 allée d'Italie, 69634 Lyon cedex, 7, France.

[††]Currently at the Applied Physics Department, Soreq Nuclear Research Center (NRC), Yavne 81800, Israel.

*Corresponding author: ryu@cars.uchicago.edu (Y-J. Ryu)

This PDF file includes:

Figs. S1 to S8

Tables S1 to S4

Supplementary figures and figure captions

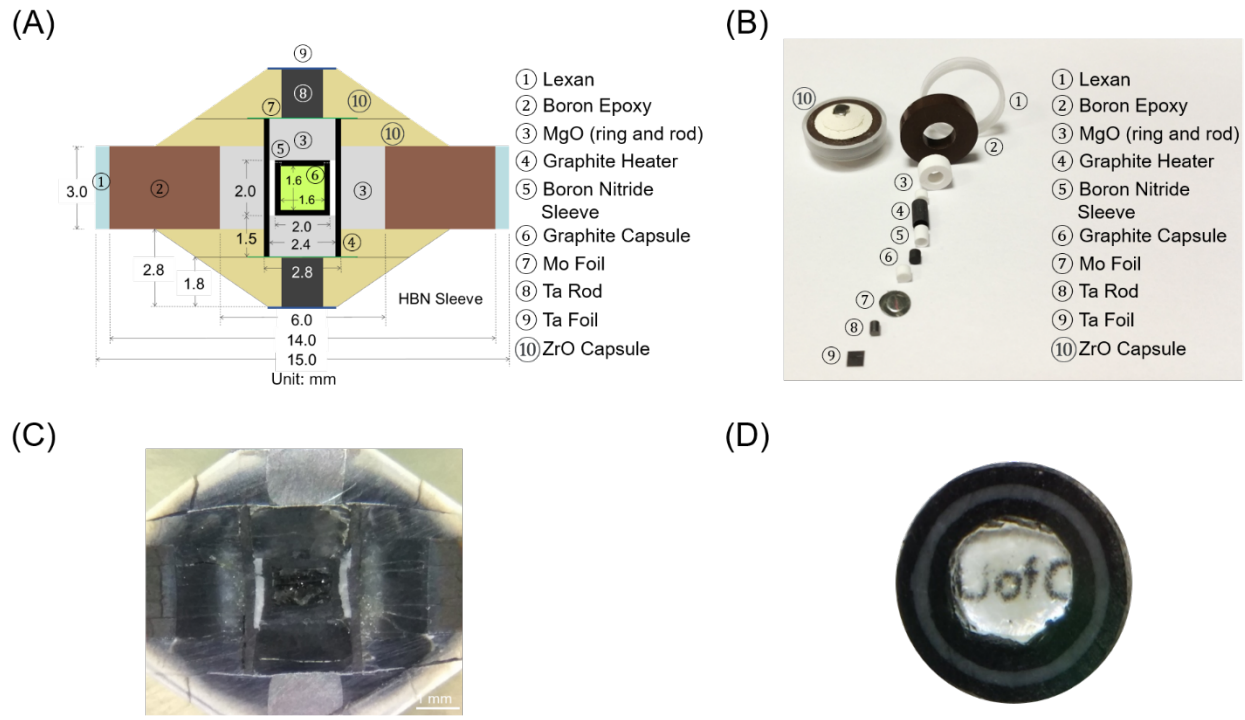

Figure S1. $MgSiO_3$ glass synthesis. (A) Schematic illustration of the cell assembly used in the Paris Edinburgh press. (B) Expanded view of the cell assembly and with actual components. (C) A photographic image of the recovered cell polished from cross section. (D) $MgSiO_3$ glass sample recovered after compressing 1:1 (MgO:SiO_2) mixture at ~1 GPa and 1600 ºC, viewed parallel to the cylindrical axis. Letters behind the $MgSiO_3$ glass are easily read. Diameter and thickness of the recovered product are both about 1mm.

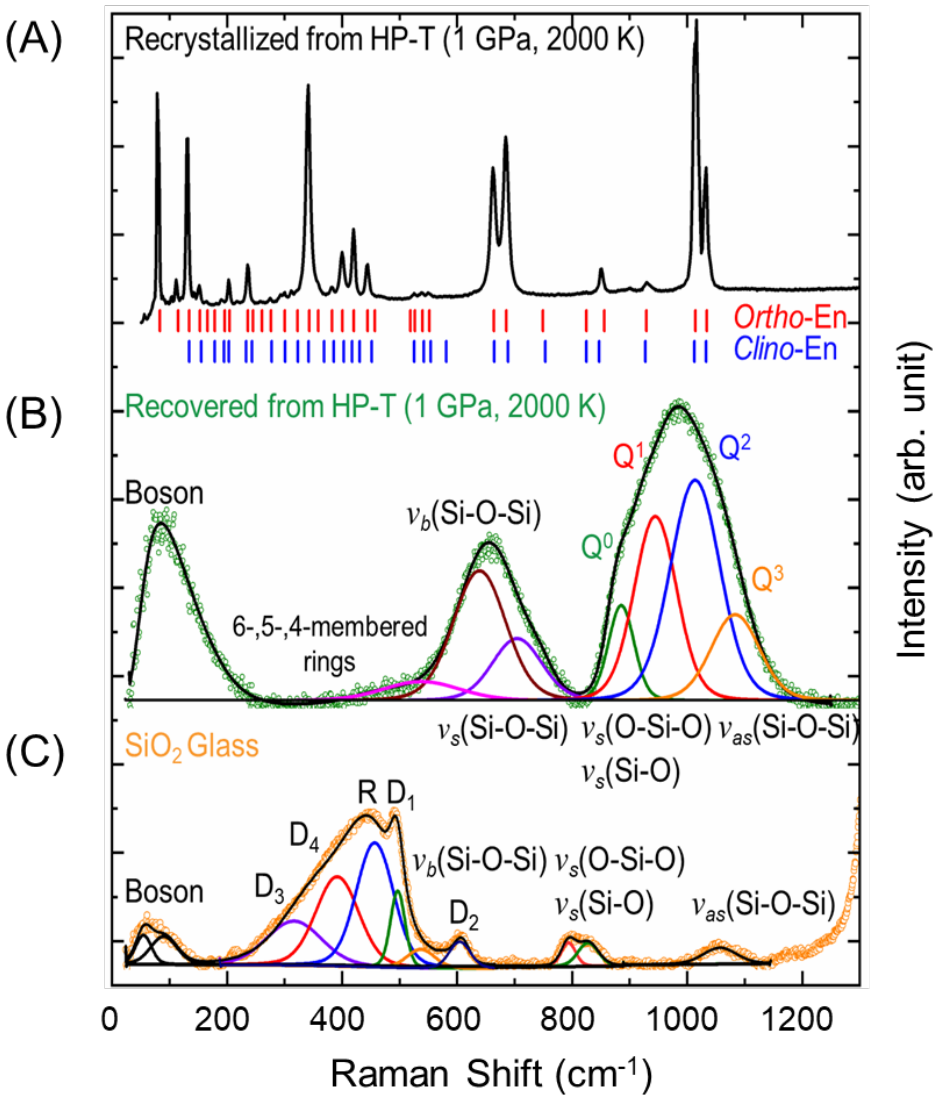

Figure S2. Raman spectra of synthesized $MgSiO_3$. (A) $MgSiO_3$ crystalline, (B) $MgSiO_3$ glass, and (C) SiO_2 glass. $MgSiO_3$ glass was made by quenching molten $MgSiO_3$. The Raman spectrum of $MgSiO_3$ glass shows a boson peak at ~100 cm^{-1}, a weak "defect peak" (dominated by 6-, 5- 4-membered rings) centered around ~530 cm^{-1}, bending and stretching Si-O-Si modes around ~600 cm^{-1}, and anti-stretching Si-O-Si mode around ~1000 cm^{-1}. All peaks are broad due to disordered nature of the glass. The anti-stretching mode (850 to 1200 cm^{-1}) can be deconvoluted into Q^n species (n=0, 1, 2, 3, 4). For comparison, the Raman spectrum of SiO_2 glass (bottom) shows D_3 (~306 cm^{-1}), D_4 (~387 cm^{-1}), D_1 (~490 cm^{-1}), D_2 (~603 cm^{-1}) modes and 6-, 5-, 4-, 3-membered rings' Raman signatures, respectively (Fu et al., 2017). The R-line (455 cm^{-1}) can be assigned to oxygen bending motion of n-membered rings with n>4.

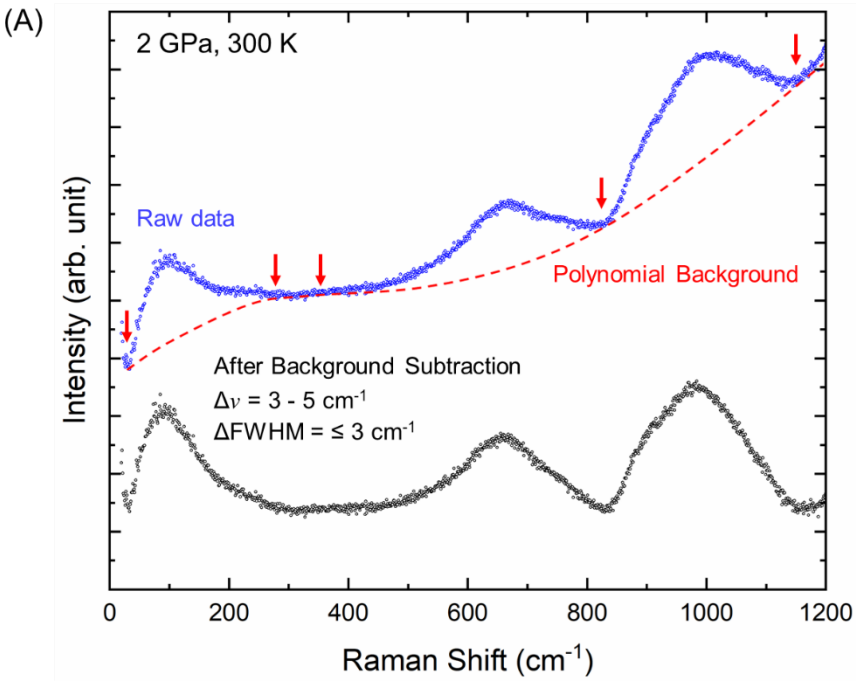

Figure S3. Background removal for the Raman spectra of $MgSiO_3$ glass. (A) The top Raman spectrum shows raw data of $MgSiO_3$ glass at 2 GPa, 300 K. Five anchor points (~30, ~250, ~330, ~800, and ~1150 cm^{-1} (red arrows)) were used to define a polynomial background. The bottom spectrum is the same data after the background subtraction. Resulted changes in peak position and FWHM after background subtraction are less than 3-5 cm^{-1}.

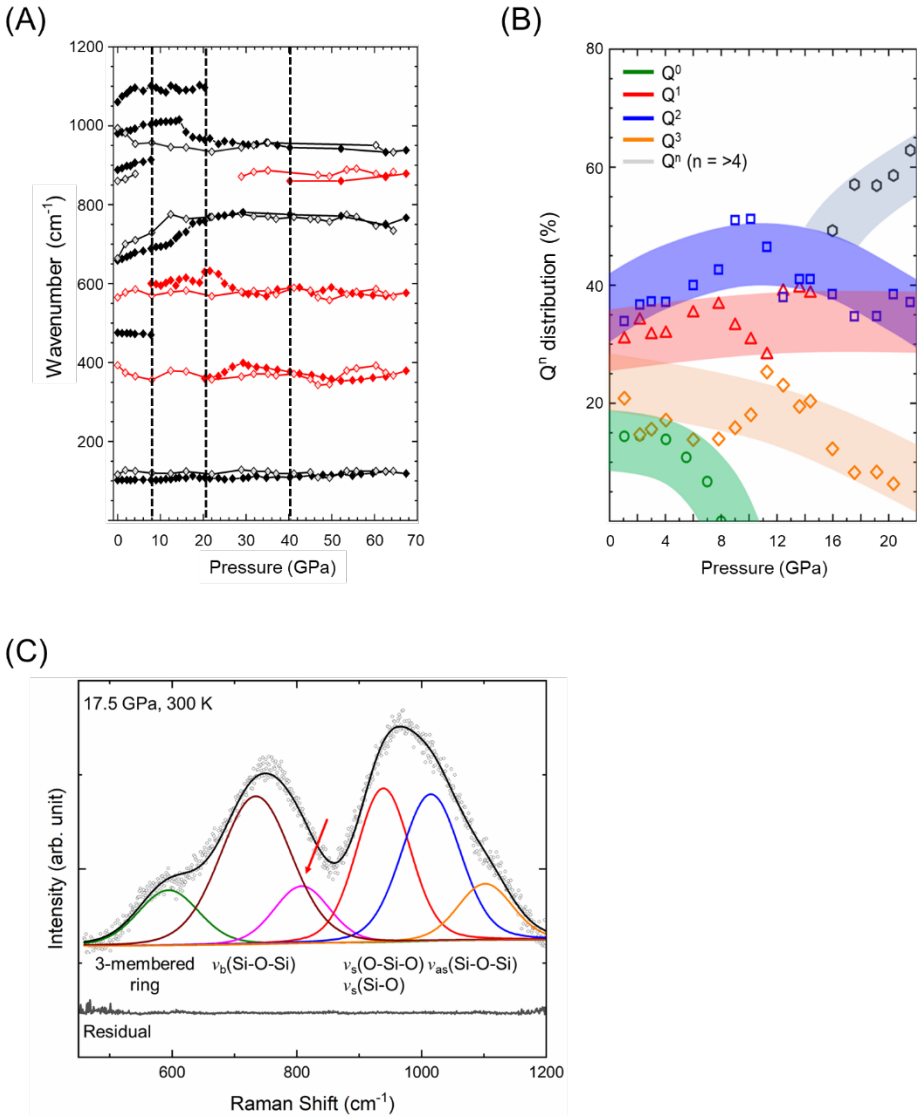

Figure S4. Details of Raman spectroscopy results over the 0 - 1300 cm^{-1} spectral range. (A) Pressure-induced Raman peak shifts of $MgSiO_3$ glass (same as Fig. 2A) showing the boson mode at ~102 cm^{-1}, 6-, 5-, 4-membered rings at 530 cm^{-1}, bending and stretching modes at 650-750 cm^{-1}, and anti-stretching mode at 850-1100 cm^{-1}. Note that the position and intensity of the boson peak are not sensitive to pressure, thus all other peaks at different pressures are normalized with respect to the boson peak at ambient conditions. (B) Pressure-induced Q^n distribution in $MgSiO_3$ glass with increasing pressure. Symbols: n=0 (green open circles), 1 (red open triangles), 2 (blue open squares), 3 (orange open diamond), >4 (grey hexagon). The shaded bands indicate uncertainty of the Q^n distribution. (C) Raman spectrum of the overlapped band (red arrow) at 17.5 GPa, showing an evidence of the presence of highly coordinated SiO_x (x=5, 6) polymorphs.

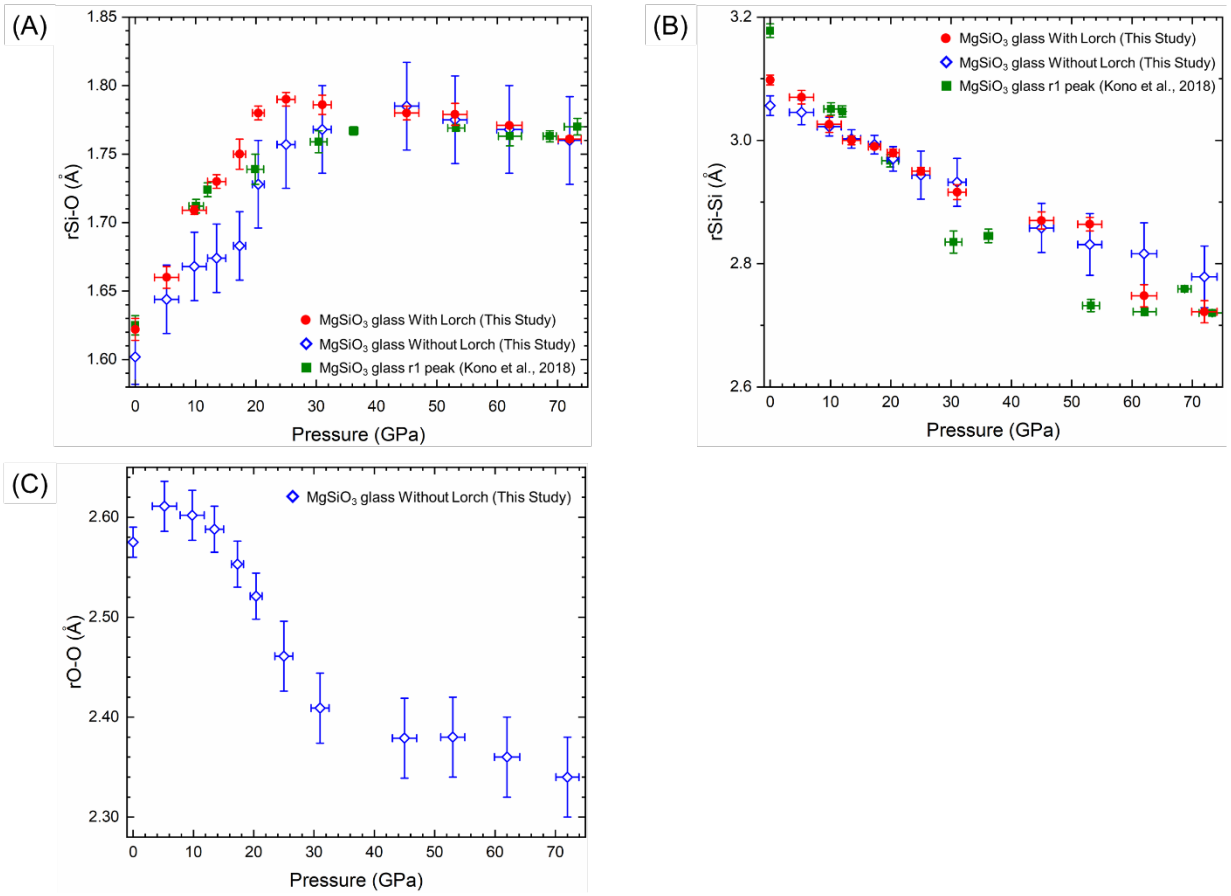

Figure S5. Bond distances extracted from pair distribution function of $MgSiO_3$ glass. (A) Pressure dependence of the Si-O bond distances (deconvoluted) obtained with (red solid circles) and without (blue empty diamonds) using the Lorch modification function. (B) Pressure dependence of the Si-Si bond distances (deconvoluted) obtained with (red solid circles) and without (blue empty diamonds) using the Lorch modification function. Green solid circles are previous experimental data from Kono et al., 2018. (C) Pressure dependence of the O-O bond distance (deconvoluted) obtained without using the Lorch modification function (blue empty diamonds).

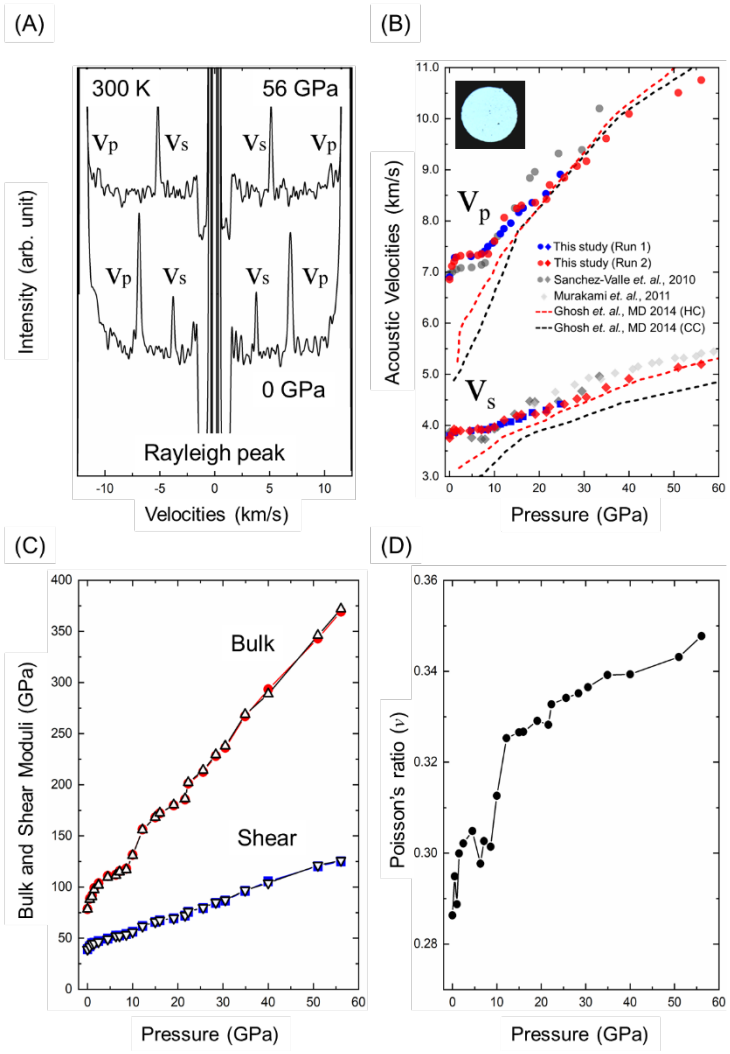

Figure S6. Pressure dependences of acoustic velocities. (A) An example of Brillouin spectra showing peaks corresponding to compressional (V_p) and shear (V_s) waves at ambient pressure (bottom) and 56 GPa (top). (B) Compressional (V_p: red and blue solid circles) and shear acoustic velocities (V_s: red and blue solid diamonds) as a function of pressure up to 56 GPa. Dark grey solid circles and diamonds represent compressional and shear velocities, respectively, from Sanchez-Valle and Bass, 2010. Pale grey solid diamonds represent shear velocities from Murakami and Bass, 2011. Red and Black dashed lines represent hot and cold compression, and shear velocities from Ghosh et al., 2014 (MD simulations). (C) The adiabatic bulk and shear moduli of $MgSiO_3$ glass as a function of pressure by using the third- (bulk: black empty triangles; shear: black empty inverse triangles) and fourth order (bulk: red solid circles; shear: blue solid squares) Birch-Murnaghan EOS of $MgSiO_3$ with previous studied density values from Petitgirard et al., 2015. Note that our density data (2.774 ± 0.014 g/cm^3) on the recovered $MgSiO_3$ glass is in good agreement with the density obtained by Petitgirard et al., 2015 (2.770 ± 0.028 g/cm^3). (D) Poisson's ratio of $MgSiO_3$ glass as a function of pressure.

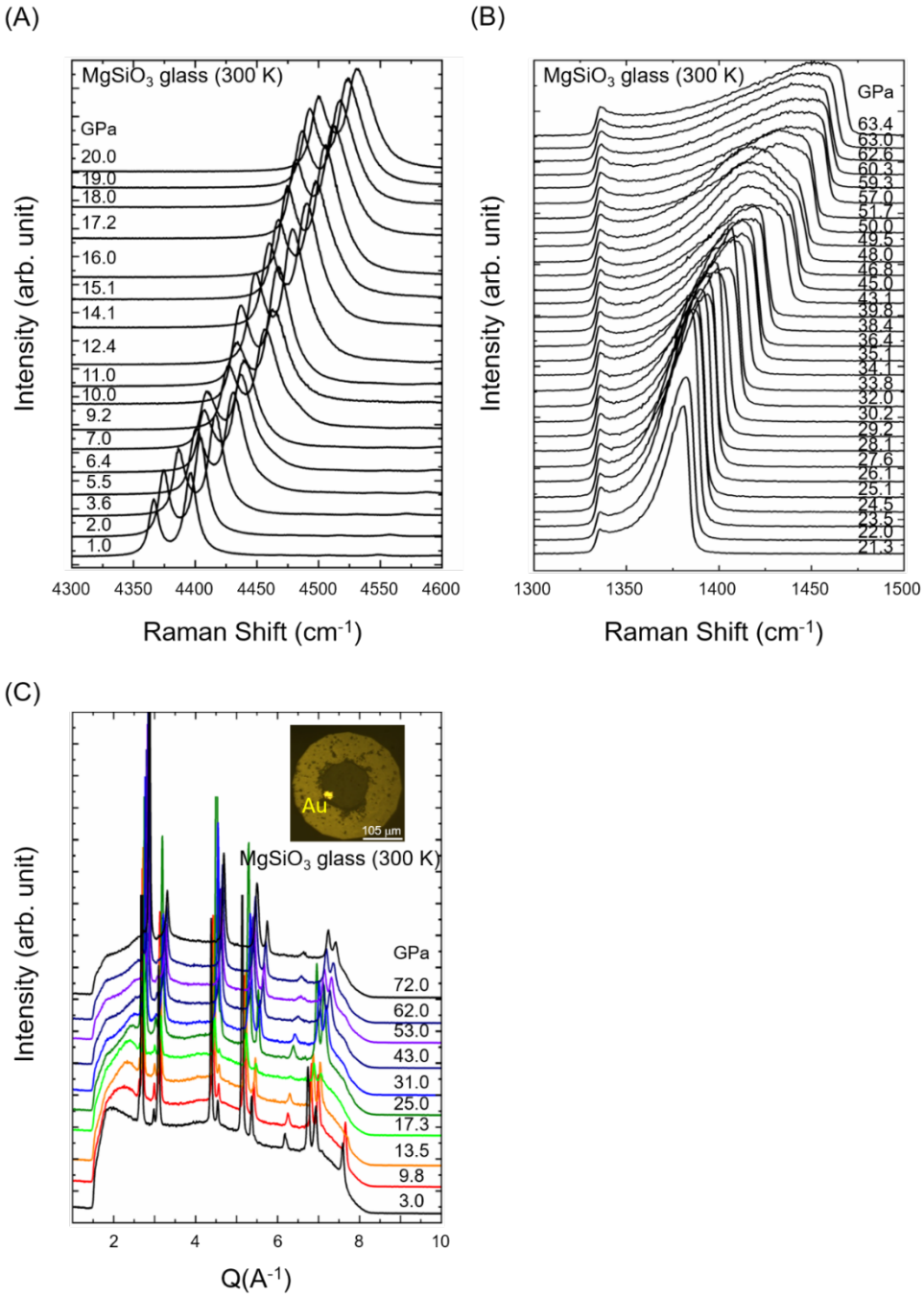

Figure S7. Pressure determination. (A) Ruby sphere (~5µm) was placed in the sample chamber to determine the pressure gradient from 0 to 20 GPa. (B) Diamond edge (Speziale et al., 2001) was used for pressure determination above 20 GPa, due to non-hydrostatic stress and pressure distribution of Ruby. (C) A gold (Au) foil (2µm x 2µm) was also placed at the edge of the sample chamber (insert), and used as a pressure calibrant in X-ray measurements, with an estimated pressure gradient about ± 1.5 to 2.0 GPa at higher pressures.

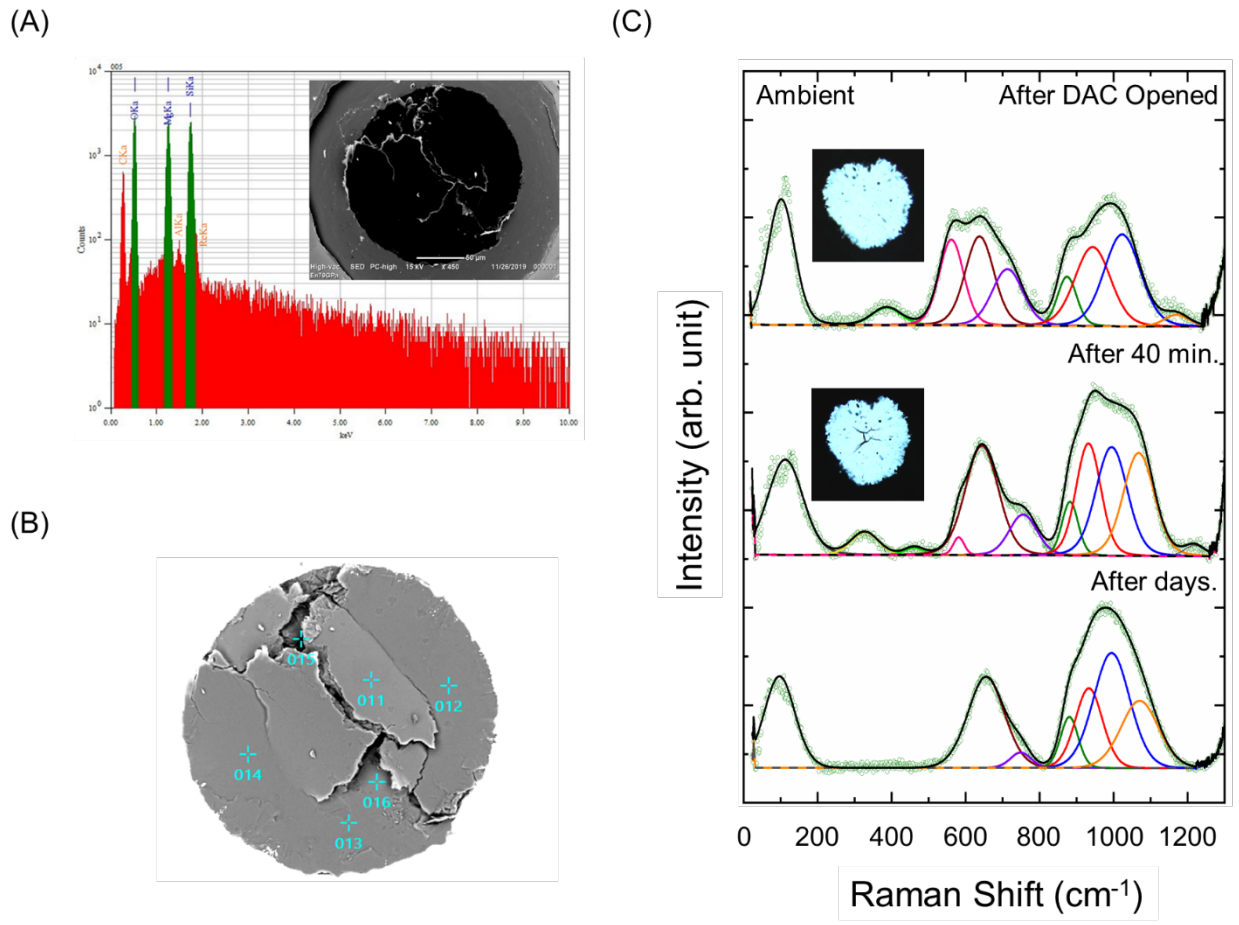

Figure S8. Energy Dispersive X-ray (EDX) analysis of $MgSiO_3$ glass on the scanning electron microscope (SEM). (A) SEM images of $MgSiO_3$ glass and (B) Image of selected $MgSiO_3$ glass areas (#11-16) for SEM-EDX analysis of the $MgSiO_3$ glass (see also, Table S4 for chemical composition analysis). (C) Raman spectra of recovered sample obtained after compression-decompression cycle. The inset shows the microphotography of recovered $MgSiO_3$ glass from high-pressure. These spectra show that the recovered sample underwent structural changes over the length of a few days at ambient pressure.

Table S1. Positions of the first and second peaks in g(r) with the Lorch modification function. The first and second maximum peak positions of rSi-O and rSi-Si were compared with Kono et al., 2018. The values are obtained with using the Lorch function by fitting the assigned peaks in g(r) with Gaussian functions.

Pressure (GPa)	1st Peak (Å)		2nd Peak (Å)	
	This Study	Kono et. al., (2018)	This Study	Kono et. al., (2018)
0	1.622 (8)	1.625 (7)	3.098 (8)	3.178 (11)
5.2 (± 0.5)	1.660 (8)	---	3.070 (11)	---
9.8 (± 0.5)	1.709 (3)	---	3.026 (13)	---
10.1 (± 1.2)	---	1.712 (5)	---	3.051 (10)
12.0 (± 0.4)	---	1.724 (5)	---	3.047 (9)
13.5 (± 0.5)	1.730 (5)	---	3.000 (7)	---
17.3 (± 1.0)	1.750 (11)	---	2.990 (4)	---
19.9 (± 1.4)	---	1.739 (11)	---	2.967 (10)
20.4 (± 1.0)	1.780 (5)	---	2.980 (6)	---
25.0 (± 1.5)	1.790 (5)	---	2.950 (6)	---
30.4 (± 1.4)	---	1.759 (8)	---	2.835 (18)
31.0 (± 1.5)	1.786 (7)	---	2.916 (12)	---
36.2 (± 0.7)	---	1.767 (3)	---	2.845 (11)
45.0 (± 2.0)	1.780 (5)	---	2.870 (14)	---
53.0 (± 2.0)	1.779 (8)	---	2.864 (11)	---
53.2 (± 1.4)	---	1.769 (2)	---	2.732 (10)
62.0 (± 2.1)	1.771 (1)		2.748 (3)	
62.1 (± 1.9)	---	1.770 (7)		2.722 (6)
72.0 (± 1.9)	1.761 (2)	---	2.722 (4)	---
73.3 (± 2.2)	---	1.759 (6)	---	2.720 (4)

Table S2. Bond distances with experimental peak positions of g(r). The bond distance of $g(r_{Si\text{-}O})$, $g(r_{Mg\text{-}O})$, $g(r_{O\text{-}O})$, $g(r_{Si\text{-}Si})$, and $g(r_{Mg\text{-}Mg})$ were obtained with and without using the Lorch modification function by deconvoluting the assigned peaks with Gaussian functions. The measured position of g(r) are compared with previous experimental and MD data (Ghosh et al., 2014; Salmon et al., 2019).

Pressure (GPa)	Si-O (Å)				Mg-O (Å)		
	This Study (With Lorch)	This Study (Without Lorch)	Salmon et al., (2019)	Ghosh et al., (2014)	This Study (Without Lorch)	Salmon et al., 2019	Ghosh et al., 2014
0	1.622 (8)	1.602 (20)	1.642 (3)	1.640	2.051 (30)	2.050	2.050
2.0 (± 0.2)	---	---	1.642 (3)	1.642	---	2.074	2.056
4.0 (± 0.2)	---	---	1.641 (3)	1.640	---	2.075	2.050
5.2 (± 2.0)	1.660 (8)	1.644 (25)	---	1.643	2.047 (30)	2.082	2.063
6.5 (± 0.2)	---	---	1.645 (3)	1.658	---	2.091	2.068
8.5 (± 0.2)	---	---	1.650 (6)	1.663	---	2.085	2.071
9.5 (± 0.2)	---	---	1.654 (4)	1.667	---	2.083	2.069
9.8 (± 2.0)	1.709 (3)	1.668 (25)	---	1.667	2.062 (30)	2.082	2.069
11.0 (± 0.2)	---	---	1.653 (4)	1.671	---	2.079	2.072
12.5 (± 0.2)	---	---	1.655 (11)	1.678	---	2.078	2.071
13.5 (± 1.5)	1.730 (5)	1.674 (25)	---	1.686	2.057 (30)	2.083	2.071
14.5 (± 0.2)	---	---	1.667 (4)	1.690	---	2.083	2.069
16.0 (± 0.2)	---	---	1.673 (5)	1.697	---	2.078	2.069
17.3 (± 1.0)	1.750 (11)	1.683 (25)	---	1.701	2.026 (35)	2.078	2.065
17.5 (± 0.2)	---	---	1.676 (7)	1.702	---	---	2.064
20.4 (± 1.0)	1.780 (5)	1.728 (25)	---	1.705	2.018 (35)	---	2.061
25.0 (± 1.5)	1.790 (5)	1.757 (32)	---	1.712	2.014 (35)	---	2.057
31.0 (± 1.5)	1.786 (7)	1.768 (32)	---	1.717	2.000 (35)	---	2.051
45.0 (± 2.0)	1.780 (5)	1.785 (32)	---	1.721	---	---	2.044
53.0 (± 2.0)	1.779 (8)	1.775 (32)	---	1.722	---	---	2.038
62.0 (± 2.1)	1.771 (1)	1.768 (32)	---	1.712	---	---	2.036
72.0 (± 1.9)	1.761 (2)	1.760 (32)	---	1.706	---	---	2.025

Pressure (GPa)	O-O (Å)		Si-Si (Å)		∠Si-O-Si (°)		∠O-Si-O (°)
	This Study (Without Lorch)	Ghosh et al., (2014)	This Study (With Lorch)	This Study (Without Lorch)	This Study (With Lorch)	This Study (Without Lorch)	This Study (Without Lorch)
0	2.575 (30)	2.697	3.098 (8)	3.056 (16)	145.5	145.1	107.0
2.0 (± 0.2)	---	2.728	---	---	---	---	---
4.0 (± 0.2)	---	2.812	---	---	---	---	---
5.2 (± 2.0)	2.611 (30)	2.835	3.070 (11)	3.045 (20)	135.2	135.6	105.1
6.5 (± 0.2)	---	2.872	---	---	---	---	---
8.5 (± 0.2)	---	2.893	---	---	---	---	---
9.5 (± 0.2)	---	2.901	---	---	---	---	---
9.8 (± 2.0)	2.602 (28)	2.897	3.026 (12)	3.022 (15)	124.6	129.9	102.5
11.0 (± 0.2)	---	2.873	---	---	---	---	---
12.5 (± 0.2)	---	2.838	---	---	---	---	---
13.5 (± 1.5)	2.588 (30)	2.795	3.000 (7)	3.002 (15)	120.2	127.5	101.2
14.5 (± 0.2)	---	2.760	---	---	---	---	---
16.0 (± 0.2)	---	2.712	---	---	---	---	---
17.3 (± 1.0)	2.553 (35)	2.712	2.990 (4)	2.993 (20)	117.4	125.5	98.6
17.5 (± 0.2)	---	2.712	---	---	---	---	---
20.4 (± 1.0)	2.521 (40)	2.696	2.980 (6)	2.943 (39)	113.7	118.5	93.7
25.0 (± 1.5)	2.461 (40)	2.672	2.950 (6)	2.932 (39)	110.9	113.7	88.9
31.0 (± 1.5)	2.409 (40)	2.636	2.916 (12)	2.858 (40)	109.4	111.9	85.8
45.0 (± 2.0)	2.379 (40)	2.604	2.870 (14)	2.831 (50)	107.4	106.3	83.5
53.0 (± 2.0)	2.380 (45)	2.580	2.864 (11)	2.831 (50)	107.2	105.7	84.1
62.0 (± 2.1)	2.360 (45)	2.556	2.748 (18)	2.816 (50)	101.7	105.5	83.7
72.0 (± 1.9)	2.340 (45)	2.540	2.722 (18)	2.778 (50)	101.2	104.2	83.3

Table S3. **Brillouin scattering results**. Run No. 1 was performed up to ~25 GPa with a thin 10 μm sized $MgSiO_3$ glass pallet. Run No. 2 was conducted up to 56 GPa with densely packed glass powder. Superscript number indicates reference: [(1)] Petitgirard, 2017.

Pressure GPa	Shear V_s (km/s)	Compression V_p (km/s)	Density (4th BM) ρ (g/cm3) [(1)]	Bulk Modulus Ks (GPa)	Shear Modulus μ (GPa)	Poisson's Ratio *v*	Young's Moduli E (GPa)
			Run #1				
0	3.801 (0)	6.901 (0)	2.774	78.7	40.1	0.282	102.8
1.1 ± 0.1	3.864 (0)	7.280 (0)	2.898	95.9	43.3	0.304	112.8
4.8 ± 0.1	3.897 (3)	7.306 (5)	3.261	108	49.5	0.301	128.9
7.1 ± 0.1	3.920 (3)	7.360 (6)	3.409	114.8	52.4	0.302	136.4
7.8 ± 0.1	3.911 (5)	7.407 (8)	3.446	118.8	52.7	0.307	137.8
8.5 ± 0.2	3.921 (5)	7.497 (8)	3.476	124.1	53.4	0.312	140.2
9.6 ± 0.2	3.972 (3)	7.565 (7)	3.535	127.9	55.8	0.31	146.1
11.3 ± 0.2	4.023 (3)	7.745 (7)	3.619	139	58.6	0.315	154.1
12.1 ± 0.2	4.050 (8)	7.848 (10)	3.657	145.3	60	0.319	158.2
13.6 ± 0.2	4.070 (10)	7.957 (8)	3.711	153	61.5	0.323	162.7
15.4 ± 0.2	4.121 (10)	8.167 (8)	3.78	166.5	64.2	0.329	170.7
16.4 ± 0.2	4.165 (5)	8.252 (8)	3.817	171.6	66.2	0.329	176
18.4 ± 0.2	4.250 (8)	8.357 (11)	3.886	177.8	70.2	0.326	186.1
21.5 ± 0.2	4.299 (5)	8.531 (8)	3.979	191.5	73.5	0.33	195.6
24.7 ± 0.2	4.417 (5)	8.909 (7)	4.072	217.2	79.4	0.337	212.4
			Run #2				
0	3.752 (0)	6.857 (0)	2.773	78.4	39	0.286	100.5
0.5 ± 0.1	3.838 (0)	7.116 (0)	2.832	87.793	41.72	0.295	108.046
1.0 ± 0.1	3.925 (3)	7.202 (3)	2.891	90.568	44.537	0.289	114.795
1.5 ± 0.1	3.896 (3)	7.288 (3)	2.96	97.323	44.933	0.3	116.821
2.5 ± 0.1	3.896 (3)	7.317 (3)	3.059	101.873	46.436	0.302	120.933
4.5 ± 0.1	3.892 (3)	7.346 (5)	3.243	109.508	49.125	0.305	128.204
6.3 ± 0.1	3.933 (15)	7.328 (8)	3.369	111.427	52.112	0.298	135.251
7.1 ± 0.1	3.911 (15)	7.352 (11)	3.41	114.756	52.152	0.303	135.873
8.6 ± 0.2	3.921 (3)	7.354 (4)	3.48	116.882	53.51	0.301	139.275
10.0 ± 0.2	3.970 (0)	7.604 (5)	3.554	130.825	56.021	0.313	147.07
12.2 ± 0.2	4.104 (10)	8.065 (16)	3.661	155.908	61.66	0.325	163.434
15.0 ± 0.2	4.183 (10)	8.243 (5)	3.767	168.085	65.918	0.327	174.891
16.0 ± 0.2	4.212 (3)	8.302 (3)	3.804	172.21	67.49	0.327	179.075
19.1 ± 0.2	4.218 (3)	8.357 (3)	3.908	180.211	69.523	0.329	184.805
21.6 ± 0.2	4.260 (3)	8.425 (3)	3.982	186.289	72.262	0.328	191.965
22.3 ± 0.2	4.358 (5)	8.704 (10)	4.005	201.989	76.06	0.333	202.733
25.6 ± 0.2	4.415 (5)	8.846 (10)	4.096	214.07	79.842	0.334	213.04
28.4 ± 0.2	4.518 (7)	9.073 (11)	4.163	229.371	84.968	0.335	226.889
30.5 ± 1.0	4.551 (5)	9.168 (11)	4.214	237.829	87.28	0.337	233.301
34.9 ± 1.5	4.742 (5)	9.612 (11)	4.305	268.674	96.807	0.339	259.279
40.0 ± 2.0	4.913 (5)	9.963 (8)	4.305	288.776	103.914	0.339	278.355
51.0 ± 2.5	5.135 (6)	10.508 (8)	4.597	345.973	121.215	0.343	325.617
56.1 ± 3.0	5.196 (6)	10.775 (8)	4.666	371.773	125.982	0.348	339.588

Table S4. Composition analysis of $MgSiO_3$ glass. The energy dispersive x-ray spectroscopy (EDXS) results show that the ratio of MgO:SiO_2 is 1:1 within an uncertainty of 5%.

Position No. 11								
Element	(keV)	Mass (%)	Sigma	Mole (%)	Compound	Mass (%)	Cation	K
O		47.73						
Mg K	1.253	24.56	0.42	50.6	MgO	40.73	8.13	46.5692
Si K	1.739	27.7	0.63	49.4	SiO_2	59.27	7.94	53.4308
Total		100		100			16.06	
Position No. 12								
Element	(keV)	Mass (%)	Sigma	Mole (%)	Compound	Mass (%)	Cation	K
O		47.9						
Mg K	1.253	23.82	0.13	49.32	MgO	39.5	7.86	45.0995
Si K	1.739	28.28	0.2	50.68	SiO_2	60.5	8.07	54.9004
Total		100		100			15.93	
Position No. 13								
Element	(keV)	Mass (%)	Sigma	Mole (%)	Compound	Mass (%)	Cation	K
O		47.77						
Mg K	1.253	24.41	0.08	50.35	MgO	40.48	8.07	46.2751
Si K	1.739	27.82	0.11	49.65	SiO_2	59.52	7.96	53.7249
Total		100		100			16.04	
Position No. 14								
Element	(keV)	Mass (%)	Sigma	Mole (%)	Compound	Mass (%)	Cation	K
O		47.76						
Mg K	1.253	24.45	0.07	50.4	MgO	40.54	8.09	46.3393
Si K	1.739	27.79	0.11	49.6	SiO_2	59.46	7.96	53.6607
Total		100		100			16.04	
Position No. 15								
Element	(keV)	Mass (%)	Sigma	Mole (%)	Compound	Mass (%)	Cation	K
O		47.84						
Mg K	1.253	24.08	0.19	49.77	MgO	39.93	7.95	45.6158
Si K	1.739	28.08	0.29	50.23	SiO_2	60.07	8.02	54.3842
Total		100		100			16.04	
Position No. 16								
Element	(keV)	Mass (%)	Sigma	Mole (%)	Compound	Mass (%)	Cation	K
O		47.89						
Mg K	1.253	23.84	0.08	49.36	MgO	39.54	7.86	45.1487
Si K	1.739	28.26	0.12	50.64	SiO_2	60.46	8.07	54.8513
Total		100		100			15.93	